IEEE Access
Multidisciplinary | Rapid Review | Open Access Journal

Received May 7, 2019, accepted May 30, 2019, date of publication June 4, 2019, date of current version June 20, 2019.

*Digital Object Identifier 10.1109/ACCESS.2019.2920632*

# Design and Development of a Novel SMA Actuated Multi-DOF Soft Robot

**CHANGXI CHENG[1], JIANXIANG CHENG[1], AND WENKAI HUANG[1,2]**

[1]School of Mechanical and Electric Engineering, Guangzhou University, Guangzhou 510006, China
[2]Center for Research on Leading Technology of Special Equipment, School of Mechanical and Electric Engineering, Guangzhou University, Guangzhou 510006, China

Corresponding author: Wenkai Huang (16796796@qq.com)

This work was supported in part by the Social Sciences and Humanities Department of the Ministry of Education of China under Grant 18YJC88002, in part by the Guangdong Provincial Key Platform and Major Scientific Research Projects under Grant 2017GXJK136, and in part by the Guangzhou Innovation and Entrepreneurship Education Project under Grant 201709P14.

**ABSTRACT** Conventional robots have shown good positioning accuracy and reliability in multiple environments. However, the robots' lack of flexibility makes them unsuitable for application in certain areas. Thus, a soft robotic system should be considered due to its adaptivity and flexibility. This paper proposes a novel shape memory alloy (SMA)-actuated multiple degrees of freedom (DOF) soft robot, which theoretically supports a maximum of nine-DOF movement and good positioning accuracy. A motion test and positioning evaluation are conducted for the proposed multi-DOF soft robot. The structural design, control method, and analysis of the kinematics and the coordinate system are also given.

**INDEX TERMS** Soft robot, shape memory alloy, neural network.

## I. INTRODUCTION

A rigid-body robot lacks flexibility and adaptivity, due to the rigid structure, which cannot be easily implemented by control algorithms. The lack of flexibility in the control and driving system can be reduced considerably in a soft robotic system. The application areas for soft robots are diverse, and include minimally invasive surgery [1]–[3], search and inspection [4], [5], and rescue [6]. Compared with rigid robots, the potential flexibility in a soft robotic system also has challenges in modeling and control methods [7]; improving the accuracy and load performance could be difficult. Soft robotics often takes inspiration from biological studies of soft animals, such as octopi, which do not have rigid skeletons, and uses this knowledge to develop robots without rigid links [8]. Examples include robots based on caterpillars [9], octopi [10], and worms [11], among others.

The appearance of smart materials, such as shape memory alloy (SMA), has suggested new ways to develop soft robots. An SMA string is usually made of titanium alloy wire, whose displacement can be controlled by heat generated by a relatively low voltage power supply. Such material contracts when electricity is applied; the ratio of the contracting force and the dead weight can be high. However, an SMA has uniform deformation and low noise. Thus, a soft robotic system can be widely applied for grippers and other mechanical systems [12]–[16].

Reference [17] shows an SMA spring-actuated robotic module made of aluminum square plates supported by universal joints, and has presented the mathematical model of the SMA spring consisting of 2 degrees of freedom. Reference [18] demonstrated a compliant mechanism actuated by SMA wires to control the orientation of an automotive mirror, and a sliding mode control was implemented to overcome the nonlinearities of the SMA. The nonlinearities of the SMA have brought great challenges in the control algorithm. Therefore, proper mathematical modeling of the SMA to unveil its laws of motion is essential to optimize its control algorithm. Studies related to the modeling and control of SMA wire have been conducted [19]. Due to the nonlinearity, control algorithms based on a mathematical model are believed to be more applicable [20]. This work presents a novel SMA-actuated controllable continuous module, as well as open-loop and close-loop control algorithms related to this design.

The rest of this paper is organized as follows: In Section II, the structural design and the coordinate system of the proposed SMA soft robot are introduced. In Section III, the control scheme of the soft robot is given. In Section IV,

The associate editor coordinating the review of this manuscript and approving it for publication was Yongping Pan.

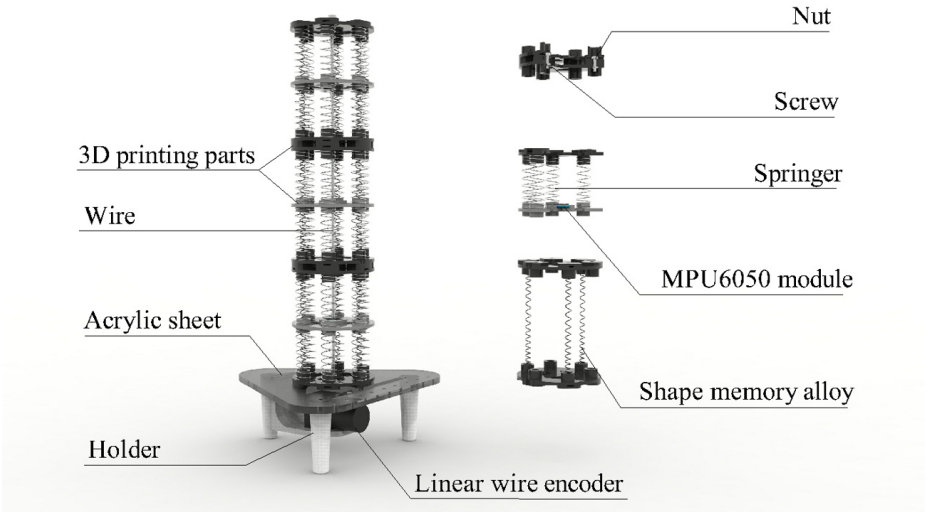


**FIGURE 1.** Schematic design of the SMA soft robot.

**TABLE 1.** Dimensions.

| | |
|---|---|
| Diameter $\Phi_1$ | 80 mm |
| Diameter $\Phi_2$ | 13 mm |
| Diameter $\Phi_3$ | 5 mm |
| Diameter $\Phi_4$ | 45 mm |
| Length $S_1$ | 115 mm |
| Length $S_2$ | 50 mm |
| Length $S_3$ | 106 mm |

an experiment with the proposed soft robot is given. In Section V, a brief conclusion is provided.

## II. DESIGN OF THE SMA SOFT ROBOT

### A. STRUCTURAL DESIGN

To realize the basic function of a soft robot, the spiral one-way SMA is adopted in this design. This type of SMA can be sketched easily by applying force, and contracted to its initial shape by heat. We designed an external circuit connected to the SMA to generate heat, and a set of springs to provide the pulling force. A schematic design of the proposed SMA shaft is shown in Fig. 1.

The whole design consists of three equal but separate units. Each unit is composed of three layers manufactured with a three-dimensional (3D) printer, where three circularly distributed SMAs connect the upper and lower layers, and six circularly distributed springs connect the center and lower layers, as well as the center and upper layers. The units are connected with a nut and a screw. With proper control of the power applied to each SMA, each unit can realize movement of 3 degrees of freedom (2 DOF of bending, 1 DOF of contracting). With a complex control method, the SMA soft robot can realize a maximum 9-DOF movement in theory. The main dimensions of each unit are listed in Table 1 and are depicted in Fig. 2.

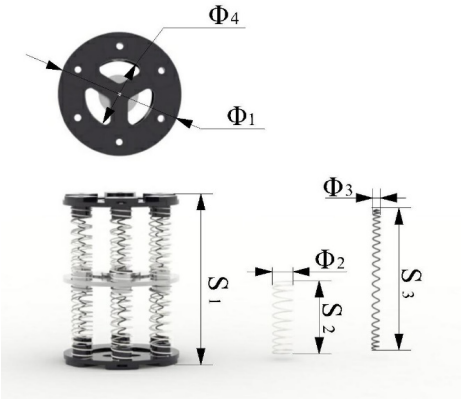


**FIGURE 2.** Dimension marking of a unit.

### B. KINEMATICS AND COORDINATE SYSTEM

The kinematics of the proposed soft robot was analyzed based on similar approach in [21], which can be described as:

The length of the midcourt line

$$\mathrm{L} = \frac{L_1 + L_2 + L_3}{3} \tag{1}$$

The bending angle

$$\beta = \frac{2\sqrt{L_1^2 + L_2^2 + L_3^2 - L_1L_2 - L_2L_3 - L_1L_3}}{3r}, \tag{2}$$

The rotating angle

$$\alpha = \tan^{-1}\left(\frac{\sqrt{3}\,(L_3 - L_2)}{L_3 + L_2 - 2L_1}\right), \tag{3}$$

The bending radius

$$\mathrm{R} = \frac{L}{\beta} = \frac{(L_1 + L_2 + L_3)\,r}{2\sqrt{L_1^2 + L_2^2 + L_3^2 - L_1L_2 - L_2L_3 - L_1L_3}}, \tag{4}$$

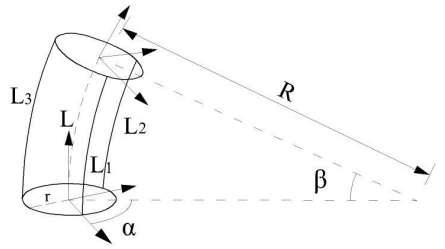


**FIGURE 3.** Three-dimensional geometric model.

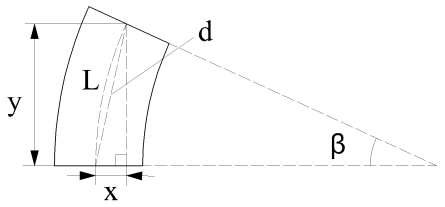


**FIGURE 4.** Two-dimensional geometric model.

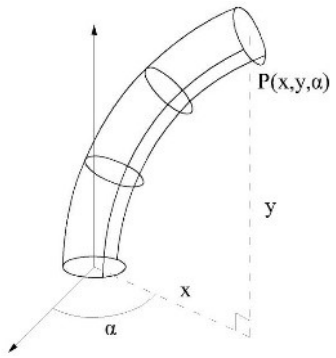


**FIGURE 5.** Coordinate system.

where $L_1$, $L_2$, $L_3$ are the lengths of each SMA wire, r is the radius of the circular base, which are marked in Fig. 3.

To position the tip of the proposed soft robot, a cylindrical-coordinate system is adopted, as shown in Fig. 5.

The tip of the soft robot can be described as P(x, y, $\alpha$), where x and y are the horizontal and vertical coordinates. $\alpha$ is the rotating angle.

As Fig. 4 shows, according to the geometry, the chord length is:

$$\mathrm{d} = 2\mathrm{R}\sin\frac{\beta}{2} \tag{5}$$

$$= \frac{(L_1+L_2+L_3)\,r}{\sqrt{L_1^2+L_2^2+L_3^2-L_1L_2-L_2L_3-L_1L_3}} \times \sin\frac{\sqrt{L_1^2+L_2^2+L_3^2-L_1L_2-L_2L_3-L_1L_3}}{3r} \tag{6}$$

For a single unit,

$$\mathrm{x} = \mathrm{d}\sin\frac{\beta}{2} \tag{7}$$

$$\mathrm{y} = \mathrm{d}\cos\frac{\beta}{2}. \tag{8}$$

In this design, the three units are controlled to move simultaneously. These units always have the same bending status. The tip point, thus, can be positioned as

$$\mathrm{P}(\mathrm{x}, \mathrm{y}, \alpha),$$

$$\mathrm{x} = 2\mathrm{R}\sin\frac{\gamma}{2}\sin\frac{\gamma}{2} \tag{9}$$

$$\mathrm{y} = 2\mathrm{R}\sin\frac{\gamma}{2}\cos\frac{\gamma}{2}, \tag{10}$$

where $\gamma = 3\beta$ is the overall bending angle.

The stiffness coefficient of a spring can be calculated as:

$$\mathrm{k} = \frac{G \times d^4}{8 \times N_c \times D_m^3}, \tag{11}$$

where $G$ is the shear modulus, $d$ is the line diameter, $N_c$is the number of active coils, and $D_m$is the pitch diameter. In this design, $G = 79000$ N/mm$^2$, $d = 0.8$ mm, $N_c = 7$, and $D_m = 13.2$ mm; k then is 0.251 N/mm. For a set consisting of 2 springs connected in series, the total stiffness would be 0.5 k. For a group of springs of the same k connected in parallel, the total stiffness is $n \times k$, where $n$ is the number of springs.

In the soft robot unit, six sets of springs are connected in parallel; each set consists of two springs, while only three sets contain SMA, namely, the actuating set. Thus, the equivalent stiffness coefficient for a pair of actuating set is $k_e$ = 0.251 N/mm.

The initial length matrix is described as

$$L_a = (L_0, L_0, L_0)\,. \tag{12}$$

The force matrix is described as

$$\mathrm{F} = (F_1, F_2, F_3)\,. \tag{13}$$

The ending length matrix after bending is

$$L_m = (L_1, L_2, L_3) = L_a - \frac{F}{k_e}. \tag{14}$$

The actuating force $F$can be controlled by applying electric power. Given the ending length matrix $L_m$ , the tip position can be determined according to (1) through (14).

When $F_1 = 3\,N, F_2 = F_3 = 0$,

The calculation results show that the displacement on the tip is 4.85 mm.

When $F_1 = 4\,N, F_2 = F_3 = 0$,

The displacement is 7.35 mm. A simulation based on these circumstances is conducted, as shown in Fig. 6.

When $\mathrm{F}_1$ =3N the edge displacement (displacement on $\mathrm{L}_1$) is 9.207mm, as shown in Fig.6 (a). the tip displacement (displacement on midcourt line L) would be approximate 4.6mm. When $\mathrm{F}_1$ =4N the edge displacement is 15.1mm, as shown in Fig.6 (b). the tip displacement would be approximate 7.5mm. The calculation result is thus verified by simulation.

## III. CONTROL SCHEME

To precisely control the contractility of each SMA, an initial test and measurement are conducted to unveil the relation of the applied power in the circuit and the contractility of the SMA, as shown in Fig. 7(a) and (b).

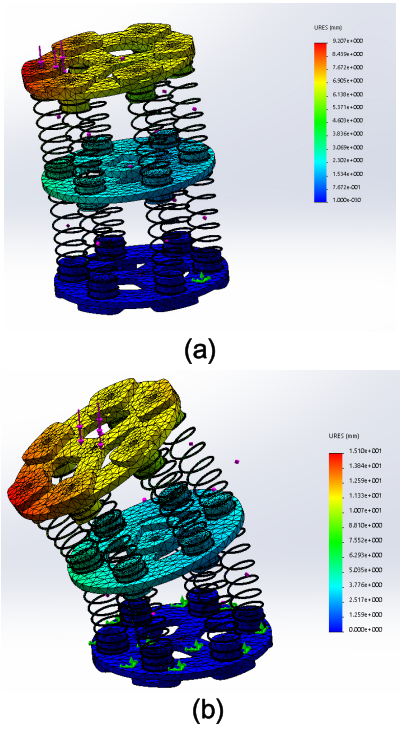


**FIGURE 6.** (a) Simulation result when $F_1 = 3N$. (b) Simulation result. when $F_1 = 4N$.

Two spring sets were designed to conduct the initial test. As Fig. 7(a) shows, set 1 was designed to measure the stiffness coefficient of the spring, and set 2 was designed to find the relation between the applied power and the contractility of a single SMA, where a metal oxide semiconductor (MOS amplifier) is included to provide the applied power. During the test, the contracting force on the SMA was found with (15):

$$F = k \times \Delta L, \tag{15}$$

In the initial test, springs of line diameter d = 1.0mm is used, where k = 0.328 N/mm is the stiffness coefficient of the spring set, and $\Delta L$ is the linear change of the spring set. The results of the initial test are depicted in Fig. 7(b). The control method was designed based on the relation unveiled in the curve.

The power on each SMA is outputted by a MOS power amplifier controlled by pulse width modulation wave (PWM) signal. The length of each SMA could thus be regulated. In addition, with the application of motion processing unit (MPU6050) and linear wire encoder (LWE), the position of the tip of the shaft can be controlled more precisely, as shown in Fig. 8(a). The overall control method is designed based on STM32 microchip controller.

The Installation of sensors and control diagram of the SMA shaft is depicted in Fig. 8. and the exact positions of the MPU and the LWE are marked in Fig. 1. Current angular position and length are gotten by the sensors and outputted to the MCU. Basic control scheme is given as follows.

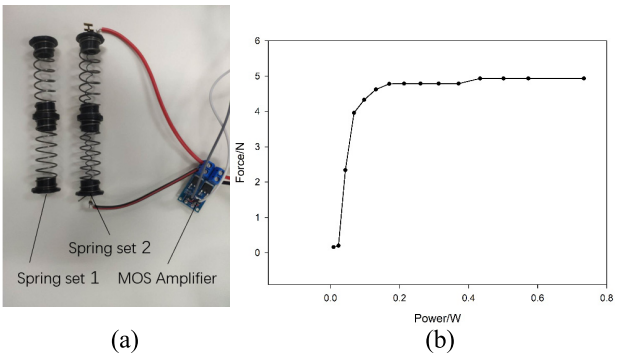


**FIGURE 7.** (a) Initial test setup. (b) Contracting force-power curve.

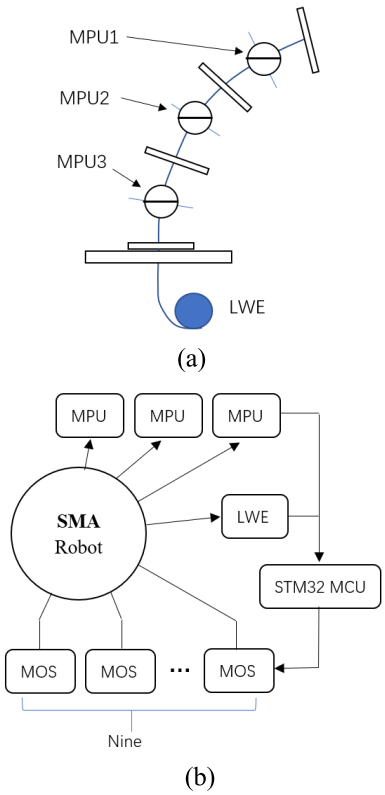


**FIGURE 8.** (a) Installation of sensors (b) Control diagram.

### A. BASIC CONTROL SCHEME

As Fig. 7(b) shows, nonlinearity appears in the curve. To extract a better algorithm to regulate the force, an additional test was conducted when the applied power ranged from 0.03 to 0.13 W. The result is shown in Fig. 9(a).

Exponential functions were adopted to fit the scatter graph, as shown in Fig. 9(b). The simple exponent exponential function, single exponential function, and double exponential function can be described as (16), (17), and (18). The fitting errors are shown in Table 2 through IV:

$$y = y_0 + a \times \left(1 - b^x\right) \tag{16}$$

$$y = y_0 + a \times \left(1 - e^{-b \cdot x}\right) \tag{17}$$

$$y = y_0 + a \times \left(1 - e^{-b \cdot x}\right) + c \times \left(1 - e^{-d \cdot x}\right). \tag{18}$$

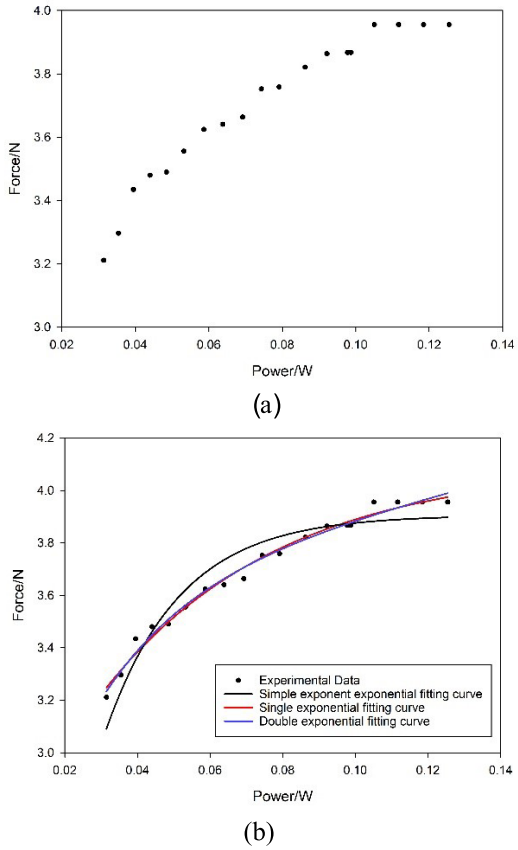


**FIGURE 9.** (a) Experiment data. (b) Fitting curve.

**TABLE 2.** Fitting errors of simple exponential function.

| | Coefficient | Std. error |
|---|---|---|
| $Y_0$ | 0.18 | 0.70 |
| a | 3.72 | 0.66 |
| b | 1.06E-21 | 1.10E-13 |

**TABLE 3.** Fitting errors of single exponential function.

| | Coefficient | Std. error |
|---|---|---|
| $Y_0$ | 2.48 | 0.11 |
| a | 1.62 | 0.08 |
| b | 20.47 | 2.61 |

where a, b, c, d are undetermined coefficients of fitting function. As Table 5 shows, a single exponential function has the lowest standard error of the estimate. In this design, a single exponential function was chosen to be the basic open-loop control algorithm, which can be expressed as:

$$P = -\frac{1}{20.47} \times \ln\left(\frac{2.48 - F}{1.62} - 1\right) \tag{19}$$

where $F$ is the target contract force, and P is the applied power. With the desired contract force set, the applied power can be determined.

**TABLE 4.** Fitting errors of double exponential function.

| | Coefficient | Std. error |
|---|---|---|
| $Y_0$ | 2.05 | 0.68 |
| a | 1043.8 | 50.15 |
| b | 0.003 | 10.13 |

**TABLE 5.** Standard error of estimate.

| | Std. error of estimate |
|---|---|
| Simple exponent exponential function | 0.0719 |
| Single exponential function | 0.0282 |
| Double exponential function | 0.0295 |

With the output power controlled by an MOS amplifier with a PWM signal, the basic open-loop control method is completed.

### *B. SIMPLIFIED ADAPTIVE NEURAL NETWORK STRUCTURE*

To improve the accuracy of the position control, a simplified adaptive neural network control algorithm is developed based on the basic open-loop algorithm.

The proposed neural network algorithm consists of three layers, namely the input layer, hidden layer and output layer, as shown in Fig.10

#### 1) INPUT LAYER

In the input layer, a neuron is included, the desired position information of the tip of the soft robot is inputted. Then the desired length $L_i$(i = 1∼9) of each actuating spring set, the desired angular position $A_1$, $A_2$, $A_3$ of each MPU sensor, the overall length of the soft robot D is outputted to the hidden layer.

#### 2) HIDDEN LAYER

In the hidden layer, five neurons are included. Neuron A contains basic open-loop algorithm, neuron $S_1$,$S_2$,$S_3$are set to regulate the angular position in each unit, where MPU1,MPU2,MPU3 are applied respectively. Neuron U is set to regulate the overall length of the soft robot, where LWE is applied.

In neuron A, the basic open-loop algorithm can be described as:

$$P_i = -\frac{1}{20.47} \times \ln\left[\frac{2.48 - k \times (L_i - L_0)}{1.62} - 1\right] \tag{20}$$

where $P_i$ (i = 1∼9) is the desired output power signal of each MOS power amplifier, $L_i$ is the desired length of each SMA, and $L_0$ is its initial length.

In neuron $S_1$,$S_2$,$S_3$, the current angular position of each unit $C_1$ $C_2$,$C_3$are gotten by MPU sensors. In neuron $S_1$, Consider axis X, when $C_{1x} > A_{1x}$, increment $X_1 = f$, $X_2 = -f$ When $C_{1x} < A_{1x}$, increment $X_1 = -f$, $X_2 = f$, else $X_1 = X_2 = 0$,

Consider axis Y, when $C_{1y} > A_{1y}$, increment $Y_3 = g$,

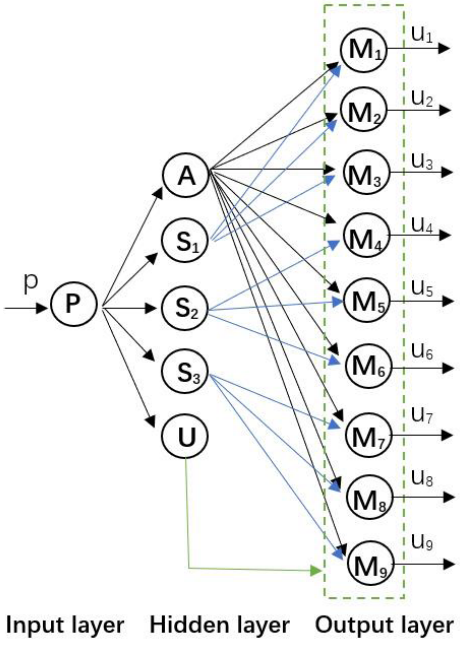


**FIGURE 10.** The simplified adaptive neural network diagram.

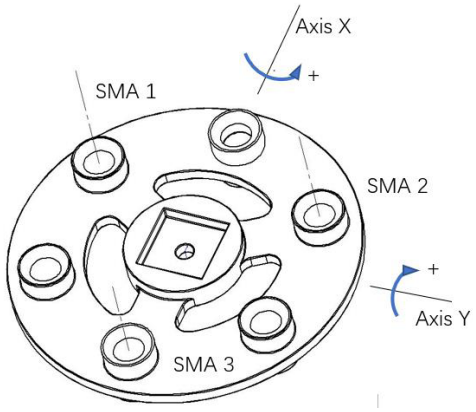


**FIGURE 11.** Definition of rotating axis.

$Y_2 = Y_1 = -$ g. When $C_{1y} < A_{1y}$, increment $Y_3 = -$ g, $Y_2 = Y_1 =$ g, else $Y_3 = Y_2 = Y_1 = 0$,

Definition of axis X and Y is given in Fig.11. Same methods are applied to neuron $S_2$ and $S_3$. Increment $X_i$and $Y_i$(I = 1∼9) are outputted to $M_i$ (i = 1∼9)in the output layer.

In neuron U, the current overall length Q is gotten by LWE.

When Q>D, increment Z = t. when Q<D, Z = − t. else Z = 0, Increment Z is outputted to $M_i$ (i = 1∼9)in the output layer. The adjusting value g, f, t could be manually set according to environmental factors.

### 3) OUTPUT LAYER

In the output layer, nine neurons $M_1 \sim M_9$ representing MOS1∼MOS9 are applied.

$$U_i = P_i + X_i + Y_i + Z \tag{21}$$

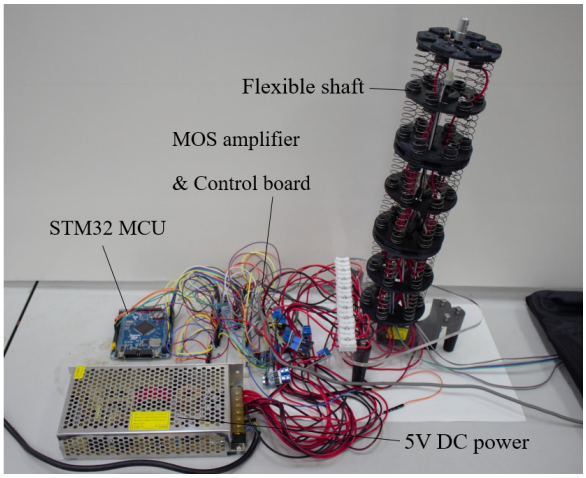


**FIGURE 12.** Experimental setup.

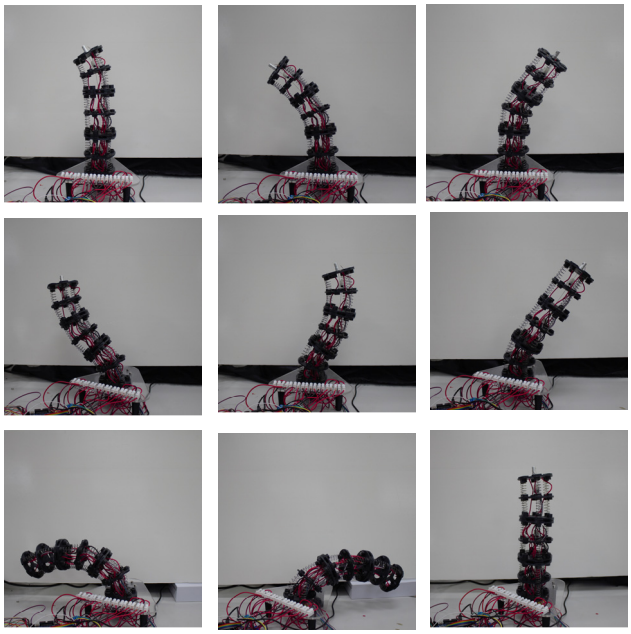

**FIGURE 13.** Different gestures of the soft robot in the motion test.

where $U_i$ (i = 1∼9) is the output power of each MOS amplifier.

### 4) LEARNING METHOD

After reaching the target position, the final value of $U_i$ will be saved as initial values in each neuron in the output layer. When the same position information is inputted to the input layer, the adaptive network will run on the basis of initial values. The initial values will be updated at each iteration.

## IV. EXPERIMENT

The multi-DOF SMA actuated soft robot is powered by 5V DC power and controlled by the STM32 MCU. Experiments are conducted on the proposed soft robot, as shown in Fig. 12.

**TABLE 6. Comparison.**

| SMA soft robot | Degree of freedom |
|---|---|
| SMA-fishing-line-Mckibben actuator [22] | 2 |
| SMA Flexible parallel manipulator [19] | 2 |
| SMA actuated continuum module [20] | 2 |
| SMA-actuated robotic module [17] | 2 |
| SMA actuated soft robot in this work | 9 |

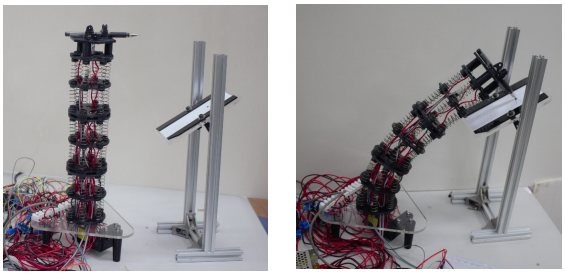

**FIGURE 14. Testing photos of the soft robot in different statuses.**

**TABLE 7. Errors of accuracy evaluation**

| | 1 | 2 | 3 | 4 | 5 | 6 | 7 | Average |
|---|---|---|---|---|---|---|---|---|
| Error/mm | 2.55 | 1.82 | 0.84 | 1.75 | 1.27 | 0.64 | 1.08 | 1.42 |

### A. MOTION TEST

Theoretically, the proposed soft robot can realize a maximum 9 degrees of freedom movement (3-DOF for each unit). A motion test was conducted on the soft robot, as shown in Fig. 13. A comparison of the soft robot in this work and other similar works is given in Table 6.

Please note that in the motion test each soft unit is controlled separately to better unveil the potential of multi-DOF motion of the proposed soft robot. The soft robot in this work can support a maximum of 9 degrees of freedom movement in theory. More than 3 degrees of freedom was verified in the motion test, which surpassed most of the current SMA actuated soft modules. With more units applied, even more degrees of freedom movement can be applied.

### B. ACCURACY EVALUATION

In the accuracy evaluation, the soft robot was driven to bend to a set spatial point to draw a dot on a fixed writing board, and then returned to its upright position. A ball pen was applied to help with the drawing, as shown in Fig. 14. The pen was driven back and forth several times to draw a series of dots to finish the evaluation. The results are listed in Table 7.

The evaluation result shows that the proposed soft robot has an average positioning error of 1.42 mm. Due to assembly error and 3D printing error, the control signal is manually adjusted. The evaluation results could serve as a reference only. With precise manufacturing methods, the positioning accuracy is expected to be better.

## V. CONCLUSION AND FUTURE WORK

The proposed soft robot is fabricated with SMA strings and regulated by MPU and LWE, which have the advantages of lightweight, adaptiveness, and controllability. Each unit supports 3 degrees of freedom movement. With the proper control method, the proposed soft robot can realize a maximum 9 degrees of freedom movement. With these advantages, the soft robot proposed in this work can be effectively adopted in tunneling, gripping, machining, and other areas, where highly adaptive soft robot systems are needed.

In this work, a non-linear function was adopted in the design of the control method. Motion sensors (MPU6050 module for the angular position and the LWE module for the linear displacement) were applied to build up the closed-loop control algorithm. In the evaluation of the positioning performance, the results showed that the proposed SMA actuated shaft had an average positioning error of 1.42 mm. In future work, sliding mode and other feedback control methods could be considered and applied to further improve the accuracy [23], [24]. In addition, external cooling methods could be implemented to shorten the recovery time.

## REFERENCES

[1] J. Burgner-Kahrs, D. C. Rucker, and H. Choset, "Continuum robots for medical applications: A survey," *IEEE Trans. Robot.*, vol. 31, no. 6, pp. 1261–1280, Dec. 2015. doi: 10.1109/TRO.2015.2489500.

[2] P. E. Dupont, J. Lock, B. Itkowitz, and E. Butler, "Design and control of concentric-tube robots," *IEEE Trans. Robot.*, vol. 26, no. 2, pp. 209–225, Apr. 2010. doi: 10.1109/TRO.2009.2035740.

[3] R. J. Webster, III, J. M. Romano, and N. J. Cowan, "Mechanics of precurved-tube continuum robots," *IEEE Trans. Robot.*, vol. 25, no. 1, pp. 67–78, Feb. 2009. doi: 10.1109/TRO.2008.2006868.

[4] I. D. Walker, "Continuous backbone 'continuum' robot manipulators," *ISRN Robot.*, vol. 2013, Jun. 2013, Art. no. 726506. doi: 10.5402/2013/726506.

[5] S. Neppalli, B. Jones, W. McMahan, V. Chitrakaran, I. Walker, M. Pritts, M. Csencsits, C. Rahn, and M. Grissom, "OctArm—A soft robotic manipulator," in *Proc. IEEE/RSJ Int. Conf. Intell. Robots Syst.*, San Diego, CA, USA, Oct./Nov. 2007, p. 2569.

[6] J. S. Mehling, M. A. Diftler, M. Chu, and M. Valvo, "A minimally invasive tendril robot for in-space inspection," in *Proc. IEEE/RAS-EMBS Int. Conf. Biomed. Robot. Biomechatron.*, Pisa, Italy, Feb. 2006, pp. 690–695.

[7] R. J. Webster, III, and B. A. Jones, "Design and kinematic modeling of constant curvature continuum robots: A review," *Int. J. Robot. Res.*, vol. 29, no. 13, pp. 1661–1683, 2010. doi: 10.1177/0278364910368147.

[8] S. Kim, C. Laschi, and B. Trimmer, "Soft robotics: A bioinspired evolution in robotics," *Trends Biotechnol.*, vol. 31, no. 5, pp. 287–294, 2013. doi: 10.1016/j.tibtech.2013.03.002.

[9] H.-T. Lin, G. G. Leisk, and B. Trimmer, "GoQBot: A caterpillar-inspired soft-bodied rolling robot," *Bioinspiration Biomimetics*, vol. 6, no. 2, 2011, Art. no. 026007. doi: 10.1088/1748-3182/6/2/026007.

[10] C. Laschi, M. Cianchetti, B. Mazzolai, L. Margheri, M. Follador, and P. Dario, "Soft robot arm inspired by the octopus," *Adv. Robot.*, vol. 26, no. 7, pp. 709–727, Apr. 2012. doi: 10.1163/156855312X626343.

[11] S. Seok, C. D. Onal, R. Wood, D. Rus, and S. Kim, "Peristaltic locomotion with antagonistic actuators in soft robotics," in *Proc. IEEE Int. Conf. Robot. Automat.*, Anchorage, AK, USA, May 2010, pp. 1228–1233.

[12] V. Farias, L. Solis, L. Melendez, C. Garcia, and R. Velazquez, "A four-fingered robot hand with shape memory alloys," in *Proc. AFRICON*, Nairobi, Kenya, 2009, pp. 1–6.

[13] S. Jung, J. Bae, and I. Moon, "Lightweight prosthetic hand with five fingers using SMA actuator," in *Proc. Int. Conf. Control, Automat. Syst. (ICCAS)*, Gyeonggi-do, South Korea, 2011, pp. 1797–1800.

[14] N. F. Rad, A. Yousefi-Koma, H. Rezaei, and M. A. Bazrafshani, "Design and fabrication of a gripper actuated by shape memory alloy spring," in *Proc. 4th Int. Conf. Robot. Mechatron. (ICROM)*, Tehran, Iran, 2016, pp. 455–458.

[15] N. Tan, X. Gu, and H. Ren, "Simultaneous robot-world, sensor-tip, and kinematics calibration of an underactuated robotic hand with soft fingers," *IEEE Access*, vol. 6, pp. 22705–22715, 2018. doi: 10.1109/ACCESS.2017.2781698.

[16] A. Al-Ibadi, S. Nefti-Meziani, and S. Davis, "Active soft end effectors for efficient grasping and safe handling," *IEEE Access*, vol. 6, pp. 23591–23601, 2018. doi: 10.1109/ACCESS.2018.2829351.

[17] A. Hadi, A. Yousefi-Koma, M. M. Moghaddam, M. Elahinia, and A. Ghazavi, "Developing a novel SMA-actuated robotic module," *Sens. Actuators A, Phys.*, vol. 162, no. 1, pp. 72–81, Jul. 2010. doi: 10.1016/j.sna.2010.06.014.

[18] E. A. Williams, G. Shaw, and M. Elahinia, "Control of an automotive shape memory alloy mirror actuator," *Mechatronics*, vol. 20, no. 5, pp. 527–534, Aug. 2010. doi: 10.1016/j.mechatronics.2010.04.002.

[19] P. R. Ranjith, G. Murali, and M. Gopal, "Modeling and simulation of a shape memory alloy spring actuated flexible parallel manipulator," *Procedia Comput. Sci.*, vol. 133, pp. 895–904, Jan. 2018. doi: 10.1016/j.procs.2018.07.104.

[20] A. Hadi, H. Akbari, B. Tarvirdizadeh, and K. Alipour, "Corrigendum to 'Developing a novel continuum module actuated by shape memory alloys,"' *Sens. Actuators A, Phys.*, vol. 247, no. 15, p. 671, Aug. 201. doi: 10.1016/j.sna.2016.06.032.

[21] L. A. T. Al Abeach, S. Nefti-Meziani, and S. Davis, "Design of a variable stiffness soft dexterous gripper," *Soft Robot.*, vol. 4, no. 3, pp. 274–284 Sep. 201. doi: 10.1089/soro.2016.0044.

[22] C. Q. Xiang, J. L. Guo, Y. Chen, L. N. Hao, and S. Davis, "Development of a SMA-fishing-line-McKibben bending actuator," *IEEE Access*, vol. 6, pp. 27183–27189, 2018. doi: 10.1109/ACCESS.2018.2830314.

[23] B. Xu, D. Yang, Z. Shi, Y. Pan, B. Chen, and F. Sun, "Online recorded data-based composite neural control of strict-feedback systems with application to hypersonic flight dynamics," *IEEE Trans. Neural Netw. Learn. Syst.*, vol. 29, no. 8, pp. 3839–3849, Aug. 2018. doi: 10.1109/TNNLS.2017.2743784.

[24] Y. Pan, Y. H. Joo, and H. Yu, "Discussions on smooth modifications of integral sliding mode control," *Int. J. Control Automat. Syst.*, vol. 16, p. 586, Apr. 2018. doi: 10.1007/s12555-017-0291-z.